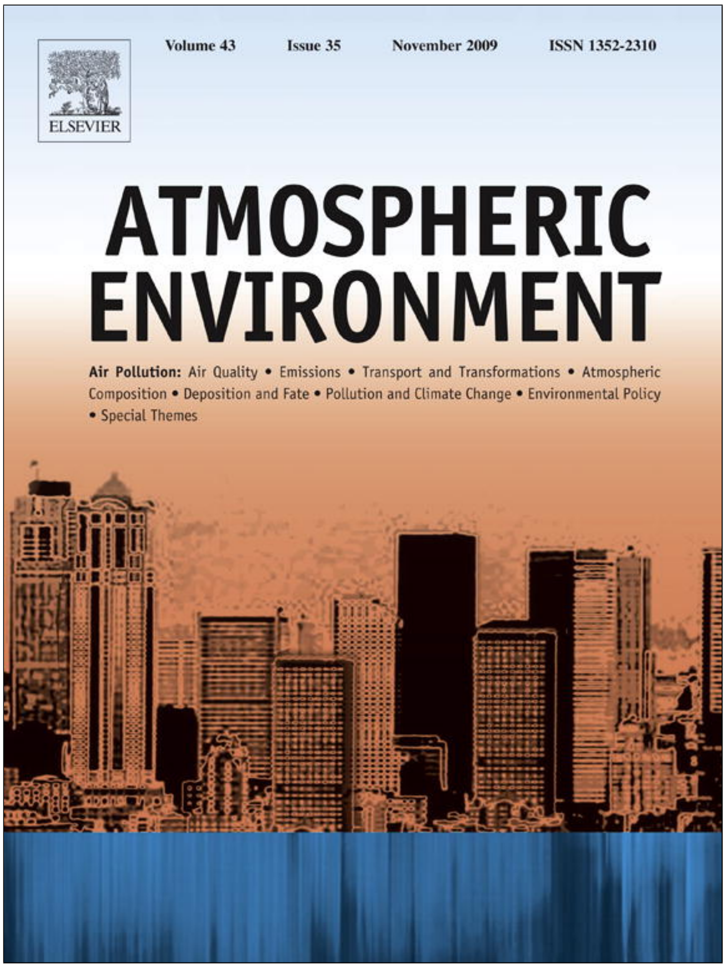
Volume 43
Issue 35
November 2009
ISSN 1352-2310
ELSEVIER
ATMOSPHERIC ENVIRONMENT
Air Pollution: Air Quality • Emissions • Transport and Transformations • Atmospheric Composition • Deposition and Fate • Pollution and Climate Change • Environmental Policy • Special Themes

Atmospheric Environment 43 (2009) 5654–5660

Contents lists available at ScienceDirect

Atmospheric Environment

journal homepage: www.elsevier.com/locate/atmosenv

Estimating bulk optical properties of aerosols over the western North Pacific by using MODIS and CERES measurements

Yong-Sang Choi [a], Chang-Hoi Ho [b], Hye-Ryun Oh [b], Rokjin J. Park [b,*], Chang-Geun Song [c]

[a] Department of Earth, Atmospheric and Planetary Sciences, Massachusetts Institute of Technology, Cambridge, MA, USA
[b] School of Earth and Environmental Sciences, Seoul National University, Seoul 151-742, Republic of Korea
[c] National Institute of Environmental Research, Incheon, Republic of Korea

ARTICLE INFO

Article history:
Received 9 April 2009
Received in revised form
22 July 2009
Accepted 24 July 2009

Keywords:
Aerosol
Radiative forcing
WNP
CERES
MODIS

ABSTRACT

Over the western North Pacific, a large amount of land aerosols from Asian-Pacific countries is transported by the prevailing westerlies. This transport makes the radiative characteristics of these aerosols diverse, particularly when one compares those characteristics over the coastal sea with those over the open sea. In this paper we discuss a method that uses satellite data to obtain the single-scattering albedo (ω) and asymmetry factor (g) of atmospheric aerosols for two large-scale subdivisions—the coastal sea (within 250 km from the coast) and the open sea (the remaining area)—over the western North Pacific (110°E–180°, 20°N–50°N). Our estimation method uses satellite measurements, obtained over a six-year period (2000–2005), of aerosol optical depth (AOD) and shortwave fluxes at both the surface and the top of the atmosphere (TOA); the measurements are obtained using the Moderate Resolution Imaging Spectroradiometer (MODIS) and the Clouds and the Earth's Radiant Energy System (CERES). For the two subdivisions, the estimated annual means of (ω, g) at 630 nm are significantly different: (0.94, 0.65) over the coastal sea and (0.97, 0.70) over the open sea. From a quantitative viewpoint, this result indicates that in comparison with aerosols over the open sea, those over the coastal sea show greater absorption and lesser forward scattering of solar radiation. The estimated optical properties are responsible for the aerosol surface cooling observed by MODIS and CERES, which is approximately 138 and 108 W m^{-2} per AOD over the coastal sea and open sea, respectively.

1. Introduction

The western North Pacific (WNP) regions are of considerable interest in climate study, because of the complex aerosol–meteorology interactions that are associated with the westerlies, frequent occurrences of synoptic waves, and highly concentrated atmospheric aerosols. Through the prevailing westerlies, a large concentration of aerosols flows from Asian continent into the WNP atmosphere. These aerosols originate from natural processes, such as biomass burning and dust storms, and also from anthropogenic processes, which have increased considerably over recent decades as a result of rapid economic growth of Asian-Pacific countries (Kaufman et al., 2002; Matsumoto et al., 2004; Choi et al., 2008). These aerosols are blended with oceanic aerosols over the WNP through atmospheric circulation (Ramanathan et al., 2001; Seinfeld et al., 2004; Bates et al., 2006). For this reason, the optical properties of aerosols over the WNP are highly variable, especially over the coastal sea (Anderson et al., 1999; Zhang et al., 2007). Therefore, to understand the effects of aerosols in radiative transfer processes, it is necessary to obtain more accurate estimates of their optical properties over the WNP in near real time (Osborne and Haywood, 2005; Bates et al., 2006; Li et al., 2007; Zhao et al., 2008).

In an attempt to estimate these aerosol optical properties, recent satellite remote sensing using visible and near-infrared bands typically produces three variables: the aerosol optical depth (AOD), the fine-mode fraction (FMF), and the Ångstrom exponent (Å). While these variables reflect the general features of aerosol mass and size distributions, a complete simulation of aerosol radiative forcing (RF) requires obtaining fundamental optical properties such as the single-scattering albedo (ω) and the asymmetry factor (g). These optical properties, however, have not yet been directly measured by spaceborne measurements, but by field experiments (Huebert et al., 2003; Jacob et al., 2003) and/or chemical transport modeling (Kim and Ramanathan, 2008; Tombette et al., 2008). The chemical modeling can fill the gaps between the limited observations and the simulated results. However, the approach using chemical modeling requires computationally large expenses, and

* Corresponding author. Tel.: +82 2 880 6715; fax: +82 2 883 4972.
E-mail address: rjpark@snu.ac.kr (R.J. Park).

1352-2310/$ – see front matter © 2009 Elsevier Ltd. All rights reserved.
doi:10.1016/j.atmosenv.2009.07.036

highly accurate physics of the chemical models; moreover, near-real-time estimation of the optical properties from the models is currently impossible.

The objective of the present study is to estimate ω and g in near real time by using satellite observations of radiative fluxes and AOD from the Moderate Resolution Imaging Spectroradiometer (MODIS) and the Clouds and the Earth's Radiant Energy System (CERES). In the merged MODIS-CERES data, the RF efficiency, defined as the ratio of aerosol RF to AOD, is available at two layers: the earth's surface and the TOA. Since the RF efficiency is theoretically a function of the two unknown values ω and g (Zhou et al., 2005), the RF efficiencies at two layers would allow one estimating ω and g values. The relation between RF efficiency and a (ω, g) pair can be obtained by a radiative transfer (RT) model in advance. Our method is a cost-efficient way for near-real-time estimates of the two values consistent physically with the spaceborne observations. Using the method, the annual and seasonal averages of aerosol properties are studied over the WNP (110°E–180° and 20°N–50°N) for nearly six years (May 2000–December 2005). We divided WNP into the coastal sea and the open sea, in consideration of regional difference in aerosol properties.

The remainder of this paper is organized as follows. Section 2 describes the satellite data and our estimation method. Section 3 introduces a general view of the aerosol distributions obtained from MODIS over the WNP. Section 4 discusses details of the estimated aerosol properties ω and g. Finally, Section 5 summarizes the findings of this study.

2. Data and method

2.1. Data

We analyzed spatial distributions of aerosols over the WNP by using AOD, FMF, and Å data obtained from the MODIS/Terra Level-3 daily gridded atmospheric data product (MOD08, collection 4). The latitude–longitude spatial resolution of the MOD08 data is $1° \times 1°$. Because 550 nm is an important wavelength that is often used in many climate modeling studies and analyses, the MODIS algorithm retrieves AOD for this wavelength by interpolating the values at 470 and 660 nm (Remer et al., 2005). It is worth noting that over the ocean, collection 4 data are not significantly different from the currently available collection 5 data (Bellouin et al., 2008). The uncertainty of the MODIS AOD data over the ocean is known to be $\pm 0.03 \pm 0.55 \times$ AOD, because of the surface reflectance, instrument calibration, and the assumptions made about aerosol properties (Levy et al., 2003; Remer et al., 2002, 2005). With AODs retrieved for wavelengths of 550 and 870 nm, respectively, the value of Å over the ocean is defined as $-\ln(AOD_{870}/AOD_{550})/\ln(870/550)$. Here, Å is averaged by means of quality-assessment weights in the MOD08 data (Hubanks et al., 2008) and is inversely proportional to the particle size. In general, high Å values ($\geq$1.0) indicate the presence of relatively smaller aerosol particles (e.g., urban pollutants and aerosols from biomass burning), and small Å values (<1.0) indicate the presence of relatively coarser aerosol particles (e.g., dust and sea-salt aerosols) (Dubovik et al., 2002). The MODIS FMF value also indicates the size distribution of aerosols, defined as the ratio of the contribution of the fine-mode AOD (i.e., with an effective aerosol radius less than 1 μm) to the total AOD. On average, the MODIS FMF value is often higher than that from airborne measurements, because the MODIS algorithm assumes that the aerosols are spherical (Levy et al., 2003; Anderson et al., 2005).

To estimate ω and g, we used the shortwave flux for the broadband frequency range of 0.3–5.0 μm, as obtained from the CERES/Terra Monthly Gridded Single Satellite Fluxes and Clouds data (FSW, edition 2C). The MODIS AOD values at 630 nm are merged over the CERES flux footprints in the FSW data, which supports the analysis of the exact relationship between the shortwave flux and the AOD. The data are available for both pristine (no clouds or aerosols in the atmosphere) and clear-sky (no clouds) conditions on a 1°-grid resolution at the surface and at the TOA. Clear-sky means that the flux footprints were made by cloud amounts less than 0.1%. We converted the fluxes from CERES-measured radiances by using surface type and cloud parameters that were averaged spatially over each region on an hourly basis. The shortwave flux has an uncertainty of 0.8 W m^{-2} at the TOA over the cloud-free region of the ocean (Wielicki et al., 1996).

2.2. Estimating the aerosol optical properties ω and g

To obtain the RF for aerosols at the surface and the TOA, we subtracted the pristine shortwave fluxes from the clear-sky shortwave fluxes in the FSW data. Note that in this RF calculation, we assumed that a given grid point was fully "contaminated" by aerosols. To calculate the RF efficiencies of aerosols at the surface and the TOA, we then divided the RF values by the total-column AOD at 630 nm in the FSW data. Given the RF efficiencies at the two levels, we could obtain values for ω and g by using the fact that the RF efficiency is a function of the two variables. To obtain the corresponding ω and g values at 630 nm, we compared the observed RF efficiencies with the simulated RF efficiencies by using an RT model. We estimated the ω and g values on a 1°-grid daily basis in the analysis domain.

The RT model used in this study is the Santa Barbara DISORT Atmospheric Radiative Transfer (SBDART) model (Ricciazzi et al., 1998), which is commonly used in satellite remote sensing of clouds and aerosols. Because they are equivalent to the FSW parameters, we simulated the clear-sky shortwave fluxes for the integrated spectral range (0.3–5.0 μm), and simulated the aerosol optical properties for the wavelength 630 nm, respectively. We scaled the assumed shortwave insolation in the SBDART model to conform to day-to-day observations of solar insolation in the FSW data. The simulation was made under the following conditions: sea water albedo; a standard midlatitude summer profile (McClatchey et al., 1972); and the presence of aerosols with various values of ω (0–1), g (0–1), and AOD (0–0.5) at intervals of 0.01. The maximum AOD is set to 0.5 because about 98% of AOD is observed below this value over the ocean. Nevertheless, given the simulated RT efficiencies, ω and g values were estimated for all grid points with AOD > 0.5. Finally, we built a look-up table that relates the simulated RF efficiencies at the surface and the TOA to ω and g.

Our study also obtained the domain-averaged ω and g values over the coastal sea (a region defined as 250 km from the coast) and the open sea (the remaining ocean area) in the analysis domain (see the line of demarcation in Fig. 1). The criterion of 250 km was determined from the seasonal variability (i.e., the time variance of the low-pass-filtered time series of a 90-day smoother) of the MODIS FMF. The coastal sea has high seasonal variability ($\geq$1.5), whereas the open sea has low seasonal variability (<1.5).

3. Characteristics of aerosols observed from MODIS

Prior to estimating the ω and g values, we examined the characteristics of aerosols over the WNP as obtained from MODIS and CERES observations. Fig. 1 shows the spatial distribution of columnar AOD, Å, and FMF retrieved from MODIS for the analysis period. The principal feature to note is that the larger values for AOD, Å, and FMF are distributed over the coastal sea and the midlatitude open sea (35°N–45°N) because of the eastward propagation of aerosols. Near the coasts, AOD is larger than 0.3 (Fig. 1a). Particularly large values for AOD (>0.4) are distributed over the

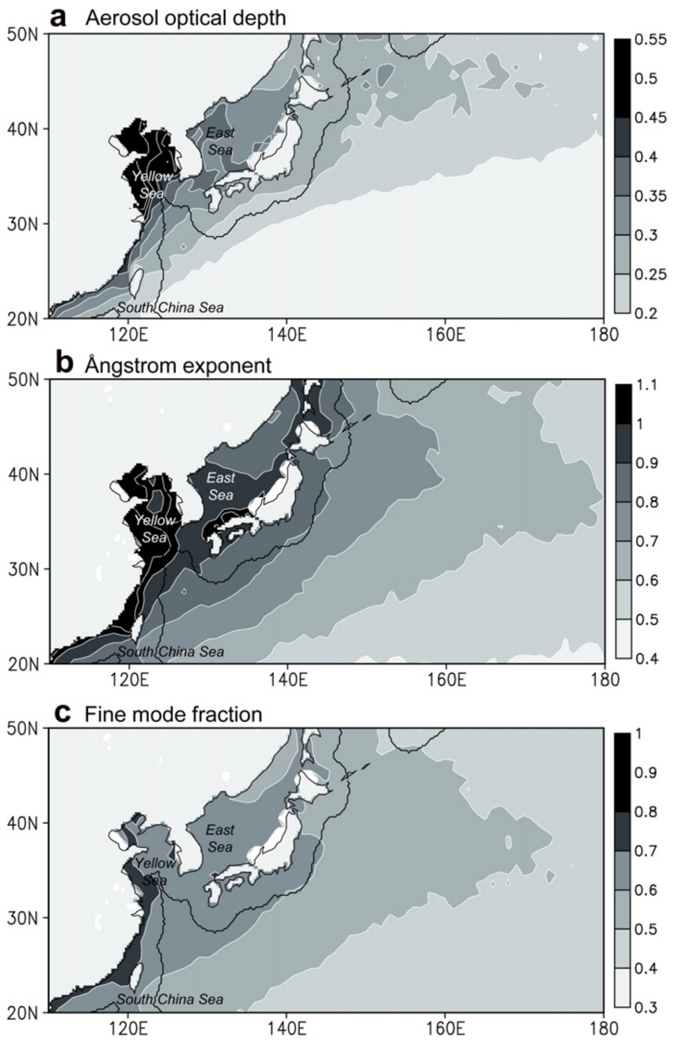

Fig. 1. MODIS-observed annual-mean aerosol optical depth (a), Ångstrom exponent (b), and fine-mode fraction (c) over the western North Pacific (110°E–180° and 20°N–50°N). The black solid line indicates the boundary of the coastal sea and the open sea.

Yellow Sea (30°N–40°N, 120°E–125°E). By contrast, AOD is generally below 0.25 over the open sea. A distribution similar to that for AOD is shown for Å and FMF (Fig. 1b and c). The highest values of Å ($\geq$1.0) and FMF ($\geq$0.7) are over the Yellow Sea and the coastward South China Sea, and relatively high Å ($\geq$0.8) and FMF ($\geq$0.6) values are dominant over the entire coastal sea. Much higher AOD, Å, and FMF values over the coastal sea indicate a massive transport of fine-mode aerosols from the land into the WNP. This provides an appropriate reason to investigate the WNP by considering separate subdivisions: the coastal sea versus the open sea.

The quantitative difference in the characteristics of aerosols over the coastal sea and over the open sea is presented as a relative frequency diagram in Fig. 2. AOD smaller than 0.2 takes about 80% of the total frequency over the open sea, while it takes about 40% over the coastal sea (Fig. 2a). By contrast, the case with AOD $\geq$ 0.2 is more frequent over the coastal sea than over the open sea. The frequency of AOD $\geq$ 0.8 is negligible over the open sea (0.9%), but it is much greater over the coastal sea (11.2%). Furthermore, the domain-averaged AOD is 0.27 over the coastal sea, and it is 0.15 over the open sea (Table 1). It is important to note that the AOD values over both regions are remarkably higher than the average AOD over the global ocean (0.07) as estimated by Christopher and Zhang (2002).

The relative frequencies of Å and FMF show different patterns than do the frequencies for AOD (Fig. 2b and c). The highest frequency is observed for Å $\geq$ 1.0 and FMF = 0.6–0.8 over the coastal sea, and for Å = 0.6–0.8 and FMF = 0.4–0.6 over the open sea. The frequency of Å $\geq$ 0.8 or FMF $\geq$ 0.6 is higher over the coastal sea than over the open sea. The domain-averaged Å value is 0.95 and 0.65 over the coastal sea and the open sea, respectively (Table 1). Furthermore, the domain-averaged FMF value is 0.66 and 0.53 over the coastal sea and the open sea, respectively. It is to be noted that the largest discrepancy between the two subdivisions is for AOD < 0.2, Å $\geq$ 1, and FMF $\geq$ 0.8. In summary, from the MODIS data, the aerosols over the coastal sea have smaller sizes and larger optical depths than those over the open sea.

The TOA and surface RF values for aerosols over the WNP from CERES observations are shown in Fig. 3. The TOA RF of aerosols over the WNP is much larger than the global ocean mean of about -5.0 W m^{-2} (Zhao et al., 2008). It is clear that the RF is stronger over the coastal sea and weaker over the open sea at both the TOA and the surface. The RF pattern is similar to that of the MODIS aerosol parameters, implying that RF is characterized mainly by the masses and types of the aerosols. However, RF has a different intensity at the two levels: at the TOA, the averaged-RF is -18.7 and -9.6 W m^{-2} over the coastal and open sea, respectively, whereas at the surface the averaged-RF is -37.3 and -16.2 W m^{-2} over the same respective regions (Table 1). The stronger RF intensity at the surface compared to that at the TOA induces a slight atmospheric warming by aerosols. This atmospheric warming is of the order of

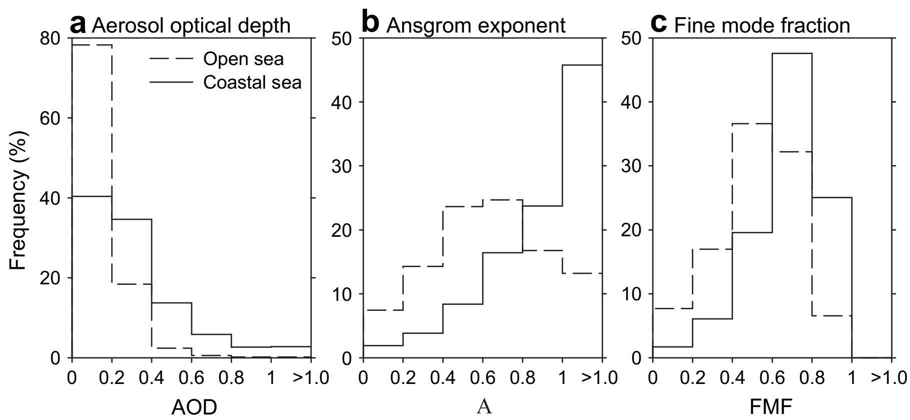

Fig. 2. Relative frequency in % of aerosol optical depth (a), Ångstrom exponent (b), and fine-mode fraction (c) over the coastal sea (solid line) and the open sea (dashed line) of the western North Pacific.

Table 1
Annual-mean aerosol characteristics over the coastal sea versus the open sea in the western North Pacific from the MODIS/CERES observations; aerosol optical depth (a), Ångstrom exponent (b), fine-mode fraction (c), radiative forcing (d), and radiative forcing efficiency (e) at the surface and the top of the atmosphere (TOA). The standard error (1σ) of the mean is given for d and e.

	Parameters		Coastal sea	Open sea
(a)	AOD		0.27	0.15
(b)	Å		0.95	0.65
(c)	FMF		0.68	0.52
(d)	RF (W m^{-2})	At the TOA	-18.61 ± 0.05	-9.61 ± 0.01
		At the surface	-37.28 ± 0.10	-16.21 ± 0.02
(e)	RF efficiency (=d/a)	At the TOA	-68.92 ± 0.19	-64.06 ± 0.08
		At the surface	-138.07 ± 0.39	-108.06 ± 0.14

18.6 and 6.6 W m^{-2} over the coastal and open sea, respectively, so that aerosols over the coastal sea have a stronger atmospheric warming effect, followed by a stronger surface-cooling effect, than over the open sea. This regional difference in RF cannot be explained by AOD alone, requiring further consideration of the effects of ω and g.

Highly concentrated aerosols over the WNP would exert a strong RF. The RF efficiency is an indication of those effects. Our analysis shows that the difference in RF efficiencies between the coastal sea and open sea is about 5 and 30 W m^{-2} AOD^{-1} at the TOA and the surface, respectively (Table 1). Clearly, there are large regional differences in the effects of ω and g with respect to light scattering and absorption at the surface than at the TOA. The possible causes are discussed using the RT model in the next section.

4. Estimating aerosol optical properties by employing the SBDART model

RT models were used to quantitatively examine the effects of ω and g on RF efficiency. These simulations are helpful in understanding the analytical relationships among RF, AOD, ω, and g. The

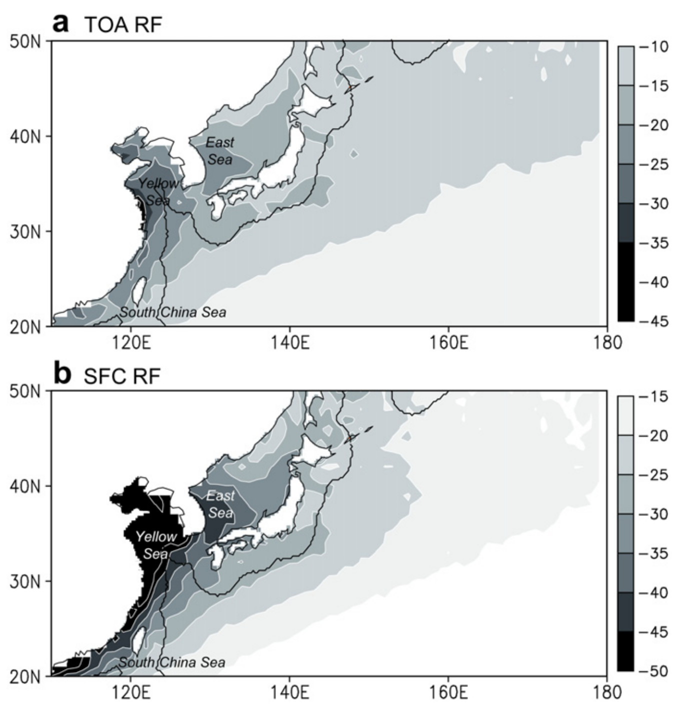

Fig. 3. Spatial distribution of the CERES-retrieved radiative forcing at the TOA (a) and surface (b) over the western North Pacific.

results of the simulation are plotted in Fig. 4. Note the linear correspondence between AOD and RF, regardless of the change in optical properties; therefore, RF efficiency can be safely defined as the slope of the line.

Fig. 4a (for a constant $g = 0.65$ and various values of ω at TOA) shows that RF decreases with an increase in ω for a given AOD. While RF is positive for $\omega < 0.6$, this positive forcing may not occur in nature, because the extent of ω is known to be 0.90–0.99 (Chin et al., 2002; Andrews et al., 2006). For cases where $\omega > 0.6$, the TOA RF is negative, and its corresponding RF efficiency ranges from -60.9 to -45.8 W m^{-2} AOD^{-1} (the slope for the shaded area). For a constant $\omega = 0.95$ and various values of g, the TOA RF increases with g (Fig. 4b). The sensitivity of RF to g is greater than it is to ω, indicating that the scattering direction is more important than the scattering quantity at the TOA. It is to be noted that $g = 0.0$ means Rayleigh scattering, in which the strongest negative forcing is simulated. On the other hand, aerosols that are completely forward scattering ($g = 1.0$) have negligible forcing, because solar light penetrates the aerosol layer in the same direction. However, the extent of g is known to be 0.45–0.80 (Chin et al., 2002; Andrews et al., 2006), and the corresponding TOA RF efficiency is between -99.0 and -20.6 W m^{-2} AOD^{-1} (the slope for the shaded area).

At the surface, for a constant $g = 0.65$ and various values of ω, RF increases with ω (Fig. 4c). This is the opposite direction of the TOA RF distribution. It is theorized that completely absorbing aerosols ($\omega = 0.0$) result in a significant surface cooling of -250 W m^{-2}. For a constant $\omega = 0.95$ and various g, we found that the surface RF also increases with g (Fig. 4d). The Surface RF is less sensitive to g than it is to ω, indicating that the scattering quantity is more important than the scattering direction at the surface. The RF efficiency at the surface has a lower range than it does at the TOA (-132.4 to -79.5 W m^{-2} AOD^{-1} for $g = 0.65$, and -155.7 to -67.9 W m^{-2} AOD^{-1} for $\omega = 0.95$).

By comparing the simulated and observed RF efficiencies, we estimated the ω and g values (see Section 2.2). On average, relatively small ω (<0.96) and g (<0.65) are dominant over the coastal sea, while the opposite is true over the open sea (Fig. 5). From the RT simulation shown in Fig. 4, the smaller ω over the coastal sea would lead to weaker radiative cooling at the TOA, and stronger radiative cooling at the surface. On the other hand, the smaller g over the coastal sea would lead to stronger radiative cooling at both the TOA and the surface. Therefore, the combined effect of ω and g values is counteracted at the TOA, but it is intensified at the surface. Consequently, the TOA RF efficiency is almost the same over both the coastal and the open sea, but the surface RF efficiency is much stronger over the coastal sea than over the open sea (Table 1).

The results of our estimation are summarized in Table 2. The annual-mean (ω, g) is (0.94, 0.65) and (0.97, 0.70) for the coastal sea and the open sea, respectively. The annual mean is comparable to results from previous studies for the Pacific Ocean. For example, the ω around the East China Sea is 0.95, as obtained from the Asian Pacific Regional Aerosol Characterization Experiment (ACE-Asia) during the spring of 2001 (Markowicz et al., 2003). The ω value is also 0.95 from observations over the remote Northern Pacific (Takemura et al., 2002), as well as from simulations (Kim and Ramanathan, 2008). The value of g is 0.69 over the northern Pacific, from the simulation of Kim and Ramanathan (2008). Note that these previous results are for the wavelength 550 nm, but our result is for 630 nm. However, the difference in the spectral dependence of light absorption by aerosols differs between 630 nm and 550 nm only on the order of the second decimal place (Eck et al., 2001; Dubovik et al., 2002; McComiskey et al., 2008).

Table 2 also shows that the ω and g values vary by season. The seasonal variation is particularly obvious over the coastal sea. The ω and g values are larger in the humid season (June through August),

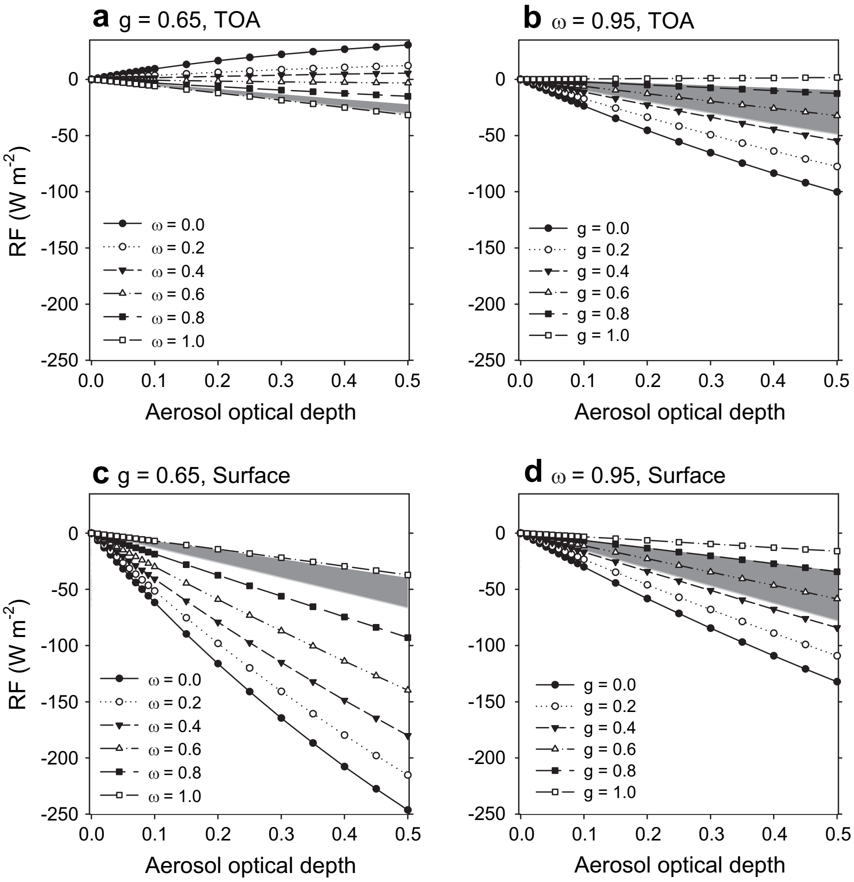

Fig. 4. Simulated radiative forcing in terms of AOD for various ω and g at the TOA (a and b) and the surface (c and d). The shaded area denotes the existent range in observations.

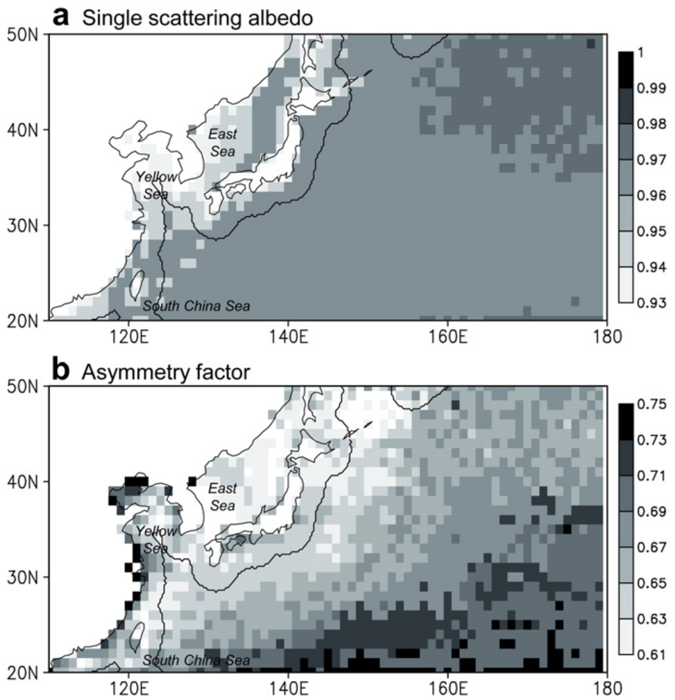

Fig. 5. Spatial distributions of the estimated annual mean ω (a) and g (b) over the western North Pacific.

and are smaller in the dry season (December through February). This may be because of the humidification effect of hygroscopic aerosols (Xia et al., 2007). The value of ω is smallest particularly in March through May, which is probably due to massive dust storms that occur in this season (Loeb and Manalo-Smith, 2005; Yan, 2007). Aerosols from frequent biomass burning in September through February may also contribute to reducing the g value over the WNP. Such significantly low g values have been reported for smoke aerosols elsewhere (Ross et al., 1998; Wong and Li, 2002).

To validate the ω and g values estimated in this study, we used the ground-based observations of the two values at 675 nm from Aerosol Robotic Network (AERONET) sites. The uncertainty of the AERONET ω and g is known to be from ±0.01 to ±0.03 and from ±0.03 to ±0.08, respectively, for all types of aerosols (Zhou et al., 2005). We selected four AERONET sites that are adjacent to the ocean and that provide consecutive data for the period of analysis: Gosan (126°E, 33°N), Osaka (135°E, 34°N), Anmyon (126°E, 36°N), and Taiwan (121°E, 25°N). These stations are all located in the

Table 2
Estimated annual and seasonal means of single-scattering albedo and asymmetry factor over the coastal sea and the open sea of the western North Pacific.

Season	Coastal sea		Open sea	
	Single-scattering albedo	Asymmetry factor	Single-scattering albedo	Asymmetry factor
Annual	0.94	0.65	0.97	0.70
MAM	0.93	0.63	0.96	0.73
JJA	0.97	0.75	0.97	0.76
SON	0.96	0.61	0.96	0.65
DJF	0.95	0.57	0.97	0.57

Table 3
Comparison of AERONET observations versus the estimations of single-scattering albedo and asymmetry factor at Gosan (a), Osaka (b), Anmyon (c), and Taiwan (d). The standard error (1σ) of the mean is also given.

Station		Sample number	Single-scattering albedo		Asymmetry factor	
			Observed value	Estimated value	Observed value	Estimated value
(a)	Gosan (126°E, 33°N)	6	–	–	0.68 ± 0.01	0.65 ± 0.01
(b)	Osaka (135°E, 34°N)	6	0.92 ± 0.02	0.93 ± 0.01	0.66 ± 0.02	0.64 ± 0.03
(c)	Anmyon (126°E, 36°N)	22	0.92 ± 0.01	0.91 ± 0.01	0.66 ± 0.01	0.61 ± 0.01
(d)	Taiwan (121°E, 25°N)	8	0.91 ± 0.02	0.94 ± 0.01	0.68 ± 0.01	0.67 ± 0.01

coastal sea area defined in this study. The AERONET level-2 data were obtained during a successful Terra overpass from 1000 through 1200 h local time (LT). We then compared the station averages with the 1°-grid averages of the daily estimates. However, because of the limited number of samples from each station, it is currently impossible to validate the daily estimates.

The results of the comparison are shown in Table 3. The estimates made by our method generally agree with the AERONET data within a bias of 0.03, with the exception of the g value from the Anmyon station. Slight upward or downward biases of ω are shown, and the downward biases of g are shown everywhere. The bias is due to a number of factors, such as different spatial resolutions, different viewing angles between the AERONET and satellite instruments, differences between the RT simulations, and other measurement uncertainties. The known uncertainties in the AOD and shortwave fluxes over the ocean are about 0.03 and 0.8 W m^{-2}, respectively. The corresponding RF uncertainty might be $\pm$1.0 W m^{-2} for AOD = 0.2. For this RF uncertainty, the tangible uncertainty in the ω and g estimates would be about 0.02. We could not investigate the exact reason and source of this bias, however, because of a lack of observations in the WNP. Nevertheless, none of the AERONET observations and the estimates of ω and g over the coastal sea are greater than the estimated annual values over the open sea (i.e., $\omega = 0.97, g = 0.70$). Therefore, the distinction between the two regions remains clear.

5. Conclusion

This study has estimated the bulk optical properties, ω and g, of aerosols over the WNP. We used the merged MODIS-CERES measurements of AOD and radiation flux for the estimation, so that the two values are physically consistent with current satellite measurements. The entire troposphere in the WNP regions displays permanent westerly flows regardless of the seasons. Consequently, massive land aerosols are continually supplied from East Asia, producing an obvious gradient of aerosol properties between those over the coastal sea and those over the open sea. Furthermore, MODIS observations indicate that AOD is higher and the aerosol size distribution is smaller over the coastal sea than over the open sea. Our estimation also shows clearly different (ω, g) values over the two subdivisions: (0.94, 0.65) over the coastal sea and (0.97, 0.70) over the open sea in the annual average. This discrepancy indicates that aerosols over the coastal sea show greater absorption and lesser forward scattering of solar radiation than do aerosols over the open sea. These estimates are comparable on average with AERONET observations, as well as with other in-situ observations and simulations made by previous studies.

The differences in ω and g of aerosols over the two regions are responsible for different surface-cooling efficiencies: -138 W m^{-2} AOD^{-1} over the coastal sea versus -108 W m^{-2} AOD^{-1} over the open sea, as obtained from the merged MODIS-CERES observations. We note that the regional difference in cooling efficiency at the TOA, however, is only 4.8 W m^{-2} AOD^{-1}. When the AOD is considered in the calculation of RF, aerosols over the coastal sea exert stronger TOA cooling than aerosols over the open sea. Consequently, the WNP regions have distinct regional differences in their aerosol optical properties, including ω, g, and AOD, and the combined effects of these different properties result in regional differences in the radiation budgets at the surface and in the atmosphere.

Because the present estimation is based purely on satellite-retrieved parameters, a near-real-time global value of aerosol optical properties is possible with this method. Moreover, the physical consistency in satellite-retrieved RF and AOD data helps ensure that estimates on a grid basis are highly accurate. A global mapping of the distribution of aerosol optical properties by this method would be helpful in understanding not only the sources and transport mechanisms of the aerosol chemical compositions, but also the radiative impact of the aerosols on both regional climates and the global climate.

Acknowledgments

This research was performed under support of "National Comprehensive Measures against Climate Change" Program by Ministry of Environment, Korea (Grant No. 1600-1637-301-210-13). Y. S. Choi was also supported by U.S. Department of Energy grant DE-FG02-01ER63257 and Korea Research Foundation grant KRF-2008-357-C00162. The authors thank the MODIS, CERES, and AERONET teams for their data.

References

Andrews, E., Sheridan, P.J., Fiebig, M., McComiskey, A., Ogren, J.A., Arnott, P., Covert, D., Elleman, R., Gasparini, R., Collins, D., Jonsson, H., Schmid, B., Wang, J., 2006. Comparison of methods for deriving aerosol asymmetry parameter. Journal of Geophysical Research 111. doi:10.1029/2004JD005734.
Anderson, T.L., Covert, D.S., Wheeler, J.D., Harris, J.M., Perry, K.D., Trost, B.E., Jaffe, D.J., Ogren, J.A., 1999. Aerosol backscatter fraction and single scattering albedo: measured values and uncertainties at a coastal station in the Pacific Northwest. Journal of Geophysical Research 104, 26793–26807.
Anderson, T., Wu, Y., Chu, D.A., Schmid, B., Redemann, J., Dubovik, O., 2005. Testing the MODIS satellite retrieval of aerosol fine-mode fraction. Journal of Geophysical Research 110. doi:10.1029/2005JD005978.
Bates, T.S., Anderson, T.L., Baynard, T., Bond, T., Boucher, O., Carmichael, G., Clarke, A., Erlick, C., Guo, H., Horowitz, L., Howell, S., Kulkarni, S., Maring, H., McComiskey, A., Middlebrook, A., Noone, K., O'Dowd, C.D., Ogren, J., Penner, J., Quinn, P.K., Ravishankara, A.R., Savoie, D.L., Schwartz, S.E., Shinozuka, Y., Tang, Y., Weber, R.J., Wu, Y., 2006. Aerosol direct radiative effects over the northwest Atlantic, northwest Pacific, and North Indian Oceans: estimates based on in situ chemical and optical measurements and chemical transport modeling. Atmospheric Chemistry and Physics 6, 1657–1732.
Bellouin, N., Jones, A., Haywood, J., Christopher, S.A., 2008. Updated estimate of aerosol direct radiative forcing from satellite observations and comparison against the Hadley Centre climate model. Journal of Geophysical Research 113. doi:10.1029/2007JD009385.
Chin, M., Ginoux, P., Kinne, S., Torres, O., Holben, B.N., Duncan, B.N., Martin, R.V., Logan, J.A., Higurashi, A., Nakajima, T., 2002. Tropospheric aerosol optical thickness from the GOCART model and comparisons with satellite and sun photometer measurements. Journal of the Atmospheric Science 59, 461–483.
Christopher, S.A., Zhang, J., 2002. Shortwave aerosol radiative forcing from MODIS and CERES observations over the oceans. Geophysical Research Letters 29. doi:10.1029/2002GL014803.
Choi, Y.S., Ho, C.H., Kim, J., Gong, D.Y., Park, R.J., 2008. The impact of aerosols on the summer rainfall frequency in China. Journal of Applied Meteorology 46, 1802–1813.
Dubovik, O., Hollben, B.N., Eck, T.F., Smirnov, A., Kaufman, Y.J., King, M.D., Tanré, D., Slutsker, I., 2002. Variability of absorption and optical properties of key aerosol types observed in worldwide locations. Journal of the Atmospheric Science 59, 590–608.
Eck, T.F., Holben, B.N., Dubovik, O., Smirnov, A., Slutsker, I., Lobert, J.M., Ramanathan, V., 2001. Column-integrated aerosol optical properties over the Maldives during the northeast monsoon for 1998–2000. Journal of Geophysical Research 106, 555–566.

Hubanks, P.A., King, M.D., Platnick, S., Pincus, R., 2008. MODIS Atmosphere L3 Gridded Product Algorithm Theoretical Basis Document. Available online at: http://modis-atmos.gsfc.nasa.gov/MOD08_D3/atbd.html.

Huebert, B.J., Bates, T., Russell, P.B., Shi, G., Kim, Y.J., Kawamura, K., Carmichael, G., Nakajima, T., 2003. An overview of ACE-Asia: strategies for quantifying the relationships between Asian aerosols and their climatic impacts. Journal of Geophysical Research 108. doi:10.1029/2003JD003550.

Jacob, D.J., Crawford, J.H., Kleb, M.M., Connors, V.S., Bendura, R.J., Raper, J.L., Sachse, G.W., Gille, J.C., Emmons, L., Heald, C.L., 2003. Transport and chemical evolution over the Pacific (TRACE-P) aircraft mission: design, execution, and first results. Journal of Geophysical Research 108. doi:10.1029/2002JD003276.

Kaufman, Y.J., Tanré, D., Boucher, O., 2002. A satellite view of aerosols in the climate system. Nature 419, 215–223.

Kim, D., Ramanathan, V., 2008. Solar radiation budget and radiative forcing due to aerosols and clouds. Journal of Geophysical Research 113. doi:10.1029/2007JD008434.

Li, Z., Xia, X., Cen, C., Holben, B.N., Wang, P., Chen, H., Tasy, S.C., Zhao, F., Dutton, E.G., Dickerson, R.E., 2007. Aerosol optical properties and their radiative effects in northern China. Journal of Geophysical Research 112. doi:10.1029/2006JD007382.

Levy, R.C., Remmer, L.A., Tanré, D., Kaufman, Y.J., Ichoku, C., Holben, B.N., Livingston, J.M., Russell, P.B., Maring, H., 2003. Evaluation of the Moderate-Resolution Imaging Spectroradiometer (MODIS) retrievals of dust aerosol over the ocean during PRIDE. Journal of Geophysical Research 108. doi:10.1029/2002JD002460.

Loeb, N.G., Manalo-Smith, N., 2005. Top-of-atmosphere direct radiative effect of aerosols over global oceans from merged CERES and MODIS observations. Journal of Climate 18, 3506–3526.

Markowicz, K.M., Flatau, J., Quinn, P.K., Carrico, C.M., Flatau, M.K., Vogelmann, A.M., Bates, D., Liu, M., Rood, M.J., 2003. Influence of relative humidity on aerosol radiative forcing: an ACE-Asia experiment perspective. Journal of Geophysical Research 108. doi:10.1029/2002JD003066.

Matsumoto, K., Uyama, Y., Hayano, T., Uematsu, M., 2004. Transport and chemical transformation of anthropogenic and mineral aerosol in the marine boundary layer over the western North Pacific Ocean. Journal of Geophysical Research 109. doi:10.1029/2004JD004696.

McClatchey, R.A., Fenn, R.W., Selby, J.E.A., Volz, F.E., Garing, J.S., 1972. Optical Properties of the Atmosphere, third ed. AFCRL Environment Research Papers 411, p. 108.

McComiskey, A., Schwartz, S.E., Schmid, B., Guan, H., Lewies, E.R., Ricchiazzi, P., Ogren, J.A., 2008. Direct aerosol forcing: calculation from observables and sensitivities to inputs. Journal of Geophysical Research 113. doi:10.1029/2007JD009170.

Osborne, S.R., Haywood, J.M., 2005. Aircraft observations of the microphysical and optical properties of major aerosol species. Atmospheric Research 73, 173–201.

Ramanathan, V., Crutzen, P.J., Kiehl, J.T., Rosenfeld, D., 2001. Aerosols, climate, and the hydrological cycle. Science 294, 2119–2124.

Remer, L.A., Tanré, D., Kaufman, Y.J., Ichoku, C., Mattoo, S., Levy, R., Chu, D.A., Holben, B., Dubovik, O., Smimov, A., Martins, J.V., Li, R.R., Ahmad, Z., 2002. Validation of MODIS aerosol retrieval over ocean. Geophysical Research Letters 29. doi:10.1029/2001GL013204.

Remer, L.A., Kaufman, Y.J., Tanre, D., Mattoo, S., Chu, D.A., Martins, J.V., Li, R.R., Ichoku, C., Levy, R.C., Kelidman, R.G., Eck, T.F., Vermote, E., Holben, B.N., 2005. The MODIS aerosol algorithm, products, and validation. Journal of the Atmospheric Science 62, 947–973.

Ricciazzi, P., Yang, S., Gautier, C., Sowle, D., 1998. SBDART: a research and teaching software tool for plane-parallel radiative transfer in the earth's atmosphere. Bulletin of the American Meteorological Society 79, 2101–2114.

Ross, J.L., Hobbs, P.V., Holben, B.N., 1998. Radiative characteristics of regional hazes dominated by smoke from biomass burning in Brazil: closure tests, and direct radiative forcing. Journal of Geophysical Research 103, 31925–31941.

Seinfeld, J.H., Carmichael, G.R., Arimoto, R., Conant, W.C., Brechtel, F.J., Bates, T.S., Cahill, T.A., Clarke, A.D., Doherty, S.J., Flatau, P.J., Huebert, B.J., Kim, J., Markowicz, K.M., Quinn, P.K., Russell, L.M., Russell, P.B., Shimizu, A., Shinozuka, Y., Song, C.H., Tang, Y., Uno, I., Vogelmann, A.M., Weber, R.J., Woo, J.H., Zhang, X.Y., 2004. ACE-Asia: regional climatic and atmospheric chemical effects of Asian dust and pollution. Bulletin of the American Meteorological Society 85, 367–380.

Takemura, T., Nakajima, T., Dubovik, O., Holben, B.N., Kinne, S., 2002. Single-scattering albedo and radiative forcing of various aerosol species with a global three-dimensional model. Journal of Climate 15, 333–352.

Tombette, M., Chazette, P., Sportisse, B., Roustan, Y., 2008. Simulation of aerosol optical properties over Europe with a 3-D size-resolved aerosol model: comparisons with AERONET data. Atmospheric Chemistry and Physics 8, 7115–7132.

Wielicki, B.A., Barkstrom, B.R., Harrison, E.F., Lee III, R.B., Smith, G.L., Cooper, J.E., 1996. Clouds and the Earth's Radiant Energy System (CERES): an earth observing system experiment. Bulletin of the American Meteorological Society 77, 853–868.

Wong, J., Li, Z., 2002. Retrieval of optical depth for heavy smoke aerosol plumes: uncertainties and sensitivities to optical properties. Journal of the Atmospheric Science 59, 250–261.

Xia, X., Chen, H., Goloub, P., Zhang, W., Chatenet, B., Wang, P., 2007. A compilation of aerosol optical properties and calculation of direct radiative forcing over an urban region in northern China. Journal of Geophysical Research 112. doi:10.1029/2006JD008119.

Yan, H., 2007. Aerosol scattering properties in northern China. Atmospheric Environment 41, 6916–6922.

Zhang, X., Zhuang, G., Guo, J., Yin, K., Zhang, P., 2007. Characterization of aerosol over the northern South China Sea during two cruises in 2003. Atmospheric Environment 41, 7821–7836.

Zhao, T.X.-P., Yu, H., Laszlo, I., Chin, M., Conant, W.C., 2008. Derivation of component aerosol direct radiative forcing at the top of atmosphere for clear-sky ocean. Journal of Quantitative Spectroscopy and Radiative Transfer 109, 1162–1186.

Zhou, M., Yu, H., Dickinson, R.E., Dubovik, O., Holben, B.N., 2005. A normalized description of the direct effect of key aerosol types on solar radiation as estimated from aerosol robotic network aerosols and moderate resolution imaging spectroradiometer albedos. Journal of Geophysical Research 110. doi:10.1029/2005JD005909.